



Anti-liquefaction performance of rubber-sand mixture for water treatment

Fei Liu^a, Xixue Tan^a, Yunkai Zhang^a, Jian Zhang^{b,*}

^aBeijing Advanced Innovation Center for Future Urban Design, School of Civil and Transportation Engineering, Beijing University of Civil Engineering and Architecture, Beijing 100044, China

^bSchool of Science, Beijing University of Civil Engineering and Architecture, Beijing 100044, China, email: yunchuangteam163.com (J. Zhang)

Received 26 August 2021; Accepted 23 September 2021

ABSTRACT

In this paper, GDS Dynamic Triaxial Tests were carried out to measure the dynamic pore water pressure and dynamic stress-strain of samples, with rubber particle size, rubber particle dosage, confining pressure and consolidation stress ratio as variables. The variation laws of anti-liquefaction performance of waste tire rubber-sand mixture (RSM) roadbed model samples under the action of different variables were researched. By comparing the anti-liquefaction performance of RSM samples under different test conditions, it was found that (1) the growth of dynamic pore water pressure of RSM samples under the action of cyclic loading could be divided into three stages. With a larger rubber particle size, the anti-liquefaction performance of the RSM samples was significantly enhanced. The anti-liquefaction performance of samples was also improved in the case of larger confining pressure and consolidation stress ratio. (2) When rubber particle content was 30%, the sand was hard to be liquefied under the action of cyclic loading. However, this method is not compliant with the actual engineering construction conditions. These conclusions are of guiding significance to engineering practices.

Keywords: Waste tire rubber particles; Anti-liquefaction performance

1. Introduction

Known as “black pollution”, waste tires refer to materials that can hardly be degraded naturally, thus causing serious damage to the natural environment. As recent years have witnessed an increasing number of waste tires along with the rapid growth of automobiles, how to recycle and dispose the waste tires in an effective and environmentally-friendly way has become difficulty to be solved by countries in the world. The waste tire rubber-sand mixture (RSM) has been used as the roadbed filling to replace part of sand because of its characteristics such as light-weight, strong permeability, high elasticity and low cost. In this case, not only is the amount of

sand reduced, but also the working performance of the roadbed under the action of cyclic loading is improved.

Currently, there are many researchers studying the use of sand improved by rubber particles.

Shalaby constructed a waste tire RSM roadbed in London to test the settlement of the roadbed under the actual traffic load, and found that both average settlement and maximum settlement of the mixture roadbed under the action of actual traffic load for 100 d are far smaller than those of the pure sand roadbed [1]. Edil [2] found through tests that the shearing strength of RSM can be significantly improved after adding rubber particles into the sand. In the shearing tests on RSM samples, Edinçlıler and Cagatay [3] revealed that the shearing strength of sand is

* Corresponding author.

mainly affected by such factors as the amount, shape and size of rubber particles mixed.

According to the RSM shearing test conducted by Li et al. [4], when the vertical pressure is zero, there is little friction resistance between sand particles and tire rubber particles. When a pressure is applied vertically, the friction resistance between rubber particles and sand particles is manifested as cohesive force, which is increased with the increase of rubber particle dosage. Mashiri et al. [5] also conducted a Triaxial Shearing Test on RSM, in which the improved “RX Constitutive Model” of RSM is obtained by the study of Ng et al. [6].

The compaction test on RSM samples conducted by Chacko et al. [7] revealed that the optimum moisture content of RSM samples is lower than that of pure sand samples, and it reaches the minimum when the rubber dosage is 15%.

Zhu studied the strength characteristics of cement and RSM samples by means of the unconfined compression test, and the results indicated that the shearing strength of the samples is significantly enhanced by adding cement into the RSM samples [8,9]. The shearing strength is the highest at a certain cement dosage (about 30%), and then it is decreased with the increase of cement dosage.

Considering the current research situation, there is a lack of research on the anti-liquefaction performance of waste tire RSM. To further study the variation laws of rubber particles in improving the anti-liquefaction performance of sand, the effects of rubber particle size, rubber particle dosage, confining pressure and consolidation stress ratio on the dynamic pore water pressure of samples were analyzed in this paper. Besides, the curves of several commonly used development models of dynamic pore water pressure were subjected to fitting analysis. Finally, conclusions that are of guiding significance for engineering practices were obtained from tests.

2. Experiment

2.1. Test equipment and functions

2.1.1. Composition of Dynamic Triaxial Testing System

The Dynamic Triaxial Testing System manufactured in UK was used in this test, whose composition is displayed

in Fig. 1. The data collection system consisted of signal receiver, axial force sensor and pore water pressure sensor. The external control system was composed of axial force controller, pressure chamber, confining pressure controller and back-pressure controller.

2.1.2. Test principles of GDS Dynamic Triaxial Apparatus

In terms of the test principles of the apparatus, the confining pressure and back-pressure were adjusted to the preset values σ_3 and P_0 using the confining pressure controller and back-pressure controller, respectively. When the confining pressure and back-pressure in each group reached the test target values, the dynamic load or static load was applied by controlling force or displacement with the operating software GDSLAP. Moreover, the GDSLAP software was employed to coordinate the relationship among confining pressure controller, back-pressure controller and axial displacement force control system, and to process the data collected by each sensor according to the preset computing mode. Finally, the data in each group generated during test were output by identifying the difference between the actual value and the target value during the test, as follows:

Assuming the initial diameter and initial height of the triaxial sample are D_0 and H_0 , respectively, the initial area A_0 and initial volume V_0 of the sample were calculated according to Eqs. (1) and (2).

$$V_0 = \frac{\pi D_0^2 H_0}{4} \tag{1}$$

$$A_0 = \frac{\pi D_0^2}{4} \tag{2}$$

With diameter, height, area and volume of the sample as D , H , A and V , respectively, the volume change of the sample can be calculated: $\Delta V = V_0 - V$. The volume change data of the back-pressure controller are the data changes of the pore water pressure, so the following formulas are further derived: actual axial force of sample: $\sigma = F/A + \sigma_3$, effective stress derived from pore water pressure: $\sigma'_3 = \sigma_3 - u_w$, effective axial stress: $\sigma' = \sigma - u_w$, axial

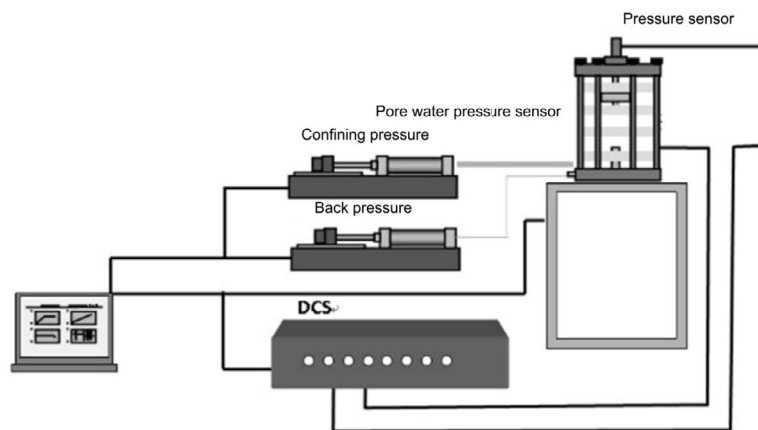


Fig. 1. The basic framework of the Dynamic Triaxial Testing System.

strain: $\varepsilon_a = (\Delta H/H_0) \times 100\%$, radial strain: $\varepsilon_r = [(-D + D_0)/D_0] \times 100\%$, and deviatoric stress obtained from effective consolidation confining pressure σ'_3 and consolidation ratio K_c : $\sigma_1 = \sigma'_3 \times K_c - \sigma'_3$.

2.2. Test schemes and failure criterion

2.2.1. Test scheme

The dynamic pore water pressure of the saturated RSM samples was tested via stress control with a sinusoidal load (stress amplitude: 30 kPa, frequency: 1 Hz and vibration times: 300). Dynamic stress, dynamic strain and dynamic pore water pressure were recorded by the GDSLAP software. When the dynamic pore water pressure reached the failure criterion or the vibration times reached 300, the experiment was stopped. The experiment scheme is shown in Table 1.

2.2.2. Failure criterion

In the dynamic pore water pressure study, the criterion of pore water pressure, that is, over-consolidation stress ratio $u_d/\sigma_3 = 1$, indicated sample failure. In other words, under the circulation of dynamic load, the pores inside the sand were compressed, and the dynamic pore water pressure between particles increased continuously. When the dynamic pore water pressure was equal to the effective confining pressure (i.e., $u_d = \sigma_3$), the effective stress among the sand particles in the samples approached zero, and the liquefaction failure of the sand occurred.

2.3. Test procedures

2.3.1. Test materials and sample preparation

- **Rubber particles.** The room-temperature pulverizing method was applied to produce rubber particles in this test. The rubber particles of three sizes (0.75, 1.5 and 2.5 mm) screened by a laboratory vibrating screen were mainly utilized (Fig. 2).
- **Sand particles.** To ensure the consistency of each group of tests, ISO standard sand (Figs. 2–5) was used as the experimental material. The density of the sand in dry state measured by density bottle method was 2.60.

- **Preparation of raw materials for Dynamic Triaxial Test samples:** Waste tire rubber particles (in three particle sizes) and Fujian standard sand. The sample preparation tools included rubber film, three-petal split mold, permeable stone and filter paper.

In order to ensure the consistent arrangement of sand particles in each group of samples, different dosages of rubber particles were added into the sand particle, so that the dry density of sand in the RSM samples kept the same as that of pure sand samples. The calculation formula is listed below:

$$\rho = \frac{M_s}{V_s + V_k} = \frac{M_0 - M_x}{V_0 - V_x} \quad (3)$$

where V_0 : total volume of RSM; V_x : volume of rubber; V_s : volume of sand; V_k : pore volume between particles; M_0 : total mass of samples; M_s : mass of sand particles; M_x : mass of rubber particles.

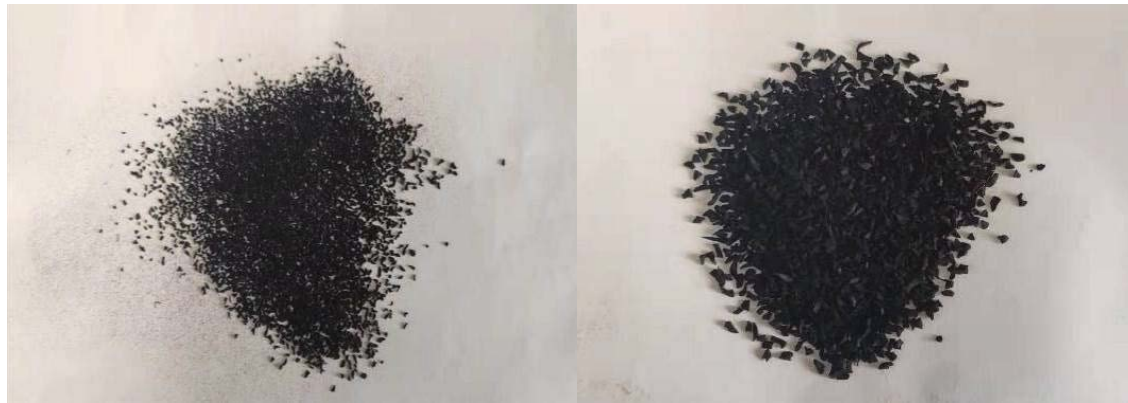
2.3.2. Sample installation, saturation and consolidation

2.3.2.1. Sample installation

The RSM samples were loaded through the moist-sampling method and weighted according to the proportion. Then the particles were boiled with water and cooled for 12 h for later use. The samples were installed after confirming the normal plug-in operation of the apparatus and no blockage of each pipe. Firstly, a permeable stone covered with a piece of wet single-layer filter paper was placed at the base of the apparatus. Secondly, the three-petal mold was installed, and the boiled and cooled RSM samples were evenly and slowly loaded into the rubber film. After that, the back-pressure was set as -30 kPa, and the three-petal mold was removed when the back-pressure loading was stable. At this time, the samples were vertical due to negative pressure. Next, the external pressure hood was installed, the apparatus was filled with water, and the numerical value of the axial force sensor was set as 0.005 kN. Then the base of apparatus was elevated to contact the top sensor. When the axial force reached 0.005 kN,

Table 1
Experimental scheme for research on dynamic pore water pressure of rubber-sand mixture

Dosage	Particle size (mm)	Consolidation stress ratio	Confining pressure (kPa)	Dynamic stress (kPa)
10%	0.75	1	50, 100, 150	30
	1.5	1, 1.5, 2	50, 100, 150	30
	2.5	1	50, 100, 150	30
20%	0.75	1	50, 100, 150	30
	1.5	1, 1.5, 2	50, 100, 150	30
	2.5	1	50, 100, 150	30
30%	0.75	1	50, 100, 150	30
	1.5	1, 1.5, 2	50, 100, 150	30
	2.5	1	50, 100, 150	30



A: 0.75 mm rubber particles; B: 1.5 mm rubber particles



C: 1.5 mm rubber particles; D: Sand used in the test

Fig. 2. Rubber particles of three sizes (0.75, 1.5 and 2.5 mm) screened.

the samples in the apparatus stopped rising to contact the axial force sensor. Finally, the vent plug at the top of the pressure chamber was removed, the inlet valve was opened to fill the pressure chamber with water, then the inlet valve was closed and the vent plug was covered.

2.3.2.2. Sample saturation

The water-head saturation and back-pressure saturation were applied to improve the saturation of RSM samples. Firstly, the water-head saturation was conducted, and the drain valve of the apparatus base was connected with the drain valve of the water container. The drain valve of the container was opened to allow the boiled and cooled distilled water to flow into the bottom of the samples from the base of the apparatus. Subsequently, the pores between the sample particles were filled with water, and the air in the samples was discharged. As the saturation of the samples was gradually increased, and the excess distilled water flowed out from the top of the samples into the prepared container. If there was still a small amount of air in the sample after the aforementioned water-head saturation, the air in the samples would be melted in water by means of five-level back-pressure saturation. Fig. 3 exhibits the variation curves of five-level back-pressure loading.

The effective confining pressure was always kept at a 20 kPa in the back-pressure loading process (the confining pressure was set greater than the back-pressure to prevent the sample preparation failure caused by the overload of dynamic pore water pressure inside the samples, and the five-level loading process could reduce the disturbance of test apparatus loading in the samples as much as possible). After the five-level back-pressure loading, the saturation of the samples was detected. A saturation condition was achieved when the B value was $\Delta u/\Delta\sigma_3 > 0.95$. If the B value failed to reach the saturation condition, the samples would be reloaded, and the saturation was detected again after the saturation processes were completed.

3. Results and discussion

3.1. Variation laws of dynamic pore water pressure of RSM samples

A dynamic stress (30 kPa) was exerted on the RSM samples using the GDS Dynamic Triaxial Apparatus, and the samples were broken down after 300 times of sustained vibration. Then the data of vibration times and dynamic pore water pressure recorded by the GD LAP system were applied to plot graphs. The variation laws of dynamic

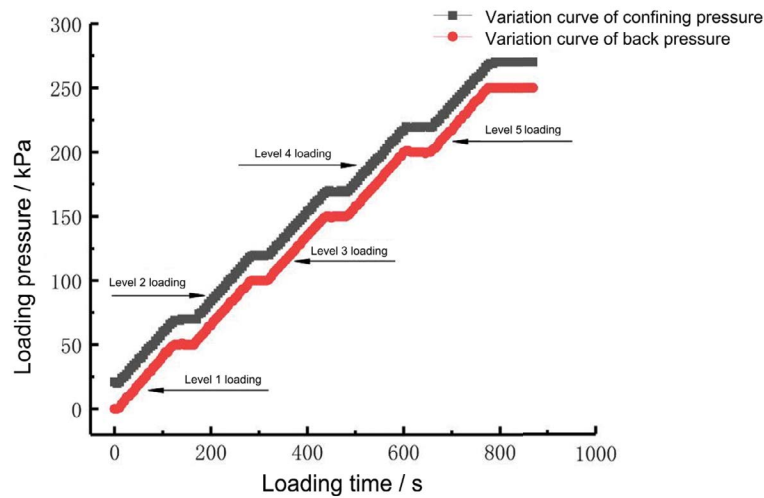


Fig. 3. Five-level loading curve of back-pressure.

pore water pressure and vibration times of the saturated RSM with different dosages of rubber particles are shown in Fig. 4.

According to the analysis on dynamic pore water pressure and vibration times of each RSM sample, the growth of dynamic pore water pressure in each group could be divided into three stages.

The first stage was the initial stage of rapid growth. The pores between particles of each sample were large within the initial vibration times of cyclic loading and later rapidly compressed by dynamic stress. In this way, the void ratio was quickly decreased, while the rapid growth of pore water pressure was observed. As shown in Fig. 4a, the trajectory of growth rate of dynamic pore water pressure in the first 25 times of vibration was closed to a straight line. Thus, the loading of 0–25 times of vibration in this test was regarded as the first stage of dynamic pore water pressure development, also known as the initial stage of rapid growth. In this stage, the growth laws of the dynamic pore water pressure of pure sand samples were similar to those of RSM samples. Specifically, the dynamic pore water pressure of pure sand samples reached 49 kPa after 25 times of dynamic stress loading and 90 kPa after 150 times of vibration, resulting in liquefaction failure of the samples.

The second stage was the middle stage of uniform growth. Most pores between sample particles in each group were filled after initial cyclic loading, and they were gradually compressed with the increasing times of vibration. As the dynamic load continued, the void ratio of samples was slowly decreased, and the dynamic pore water pressure curve was raised steadily.

The third stage was the final stable stage, also known as the stable stage of pore water pressure. The pores between sample particles were all filled, and the dynamic load on samples had a little effect on the void ratio of samples. Thus, the dynamic pore water pressure remained stable instead of growing regardless the increasing vibration times. Based on Fig. 4b, the dynamic pore water pressure of the RSM samples with a rubber dosage of 30% kept stable after 50 times

of vibration, and the final dynamic pore water pressure was far below the liquefaction criterion for samples.

Table 2 presents the effects of rubber dosage R_f and rubber particle size D_r on the anti-liquefaction performance of the sand. The anti-liquefaction performance improvement rate of the sand was calculated according to Eq. (4), in which U_d was the numerical value of dynamic pore water pressure in a steady state. The tested samples were liquefied when the liquefaction criterion U_d and effective confining pressure σ'_3 were achieved:

$$R = \frac{|U_d - \sigma'_3|}{\sigma'_3} \times 100\% \quad (4)$$

where R anti-liquefaction performance improvement rate; U_d : dynamic pore water pressure; σ'_3 : effective confining pressure.

3.1.1. Effect of rubber particle size on anti-liquefaction performance of samples

The rubber particles crushed by machine could be roughly divided into three size groups: 0.75, 1.5 and 2.5 mm. It was discovered through the test results that the samples with larger rubber particle size showed prominently enhanced anti-liquefaction performance. When the rubber particle size D_r was 2.5 mm, the anti-liquefaction performance improvement rate of the three groups of RSM samples with different rubber dosages was 12.8% ($R_f = 10\%$), 23.8% ($R_f = 20\%$) and 52.6% ($R_f = 30\%$), respectively. Moreover, the anti-liquefaction performance improvement rate reached the maximum of 52.6% when the rubber dosage was up to 30%.

The anti-liquefaction performance of the sample could be significantly improved by the rubber particles of three sizes, which could be explained by particle analog analysis. Specifically, adding large rubber particles into sand was equivalent to adding gravels into sand. In this way, the pores between sample sand were enlarged, the

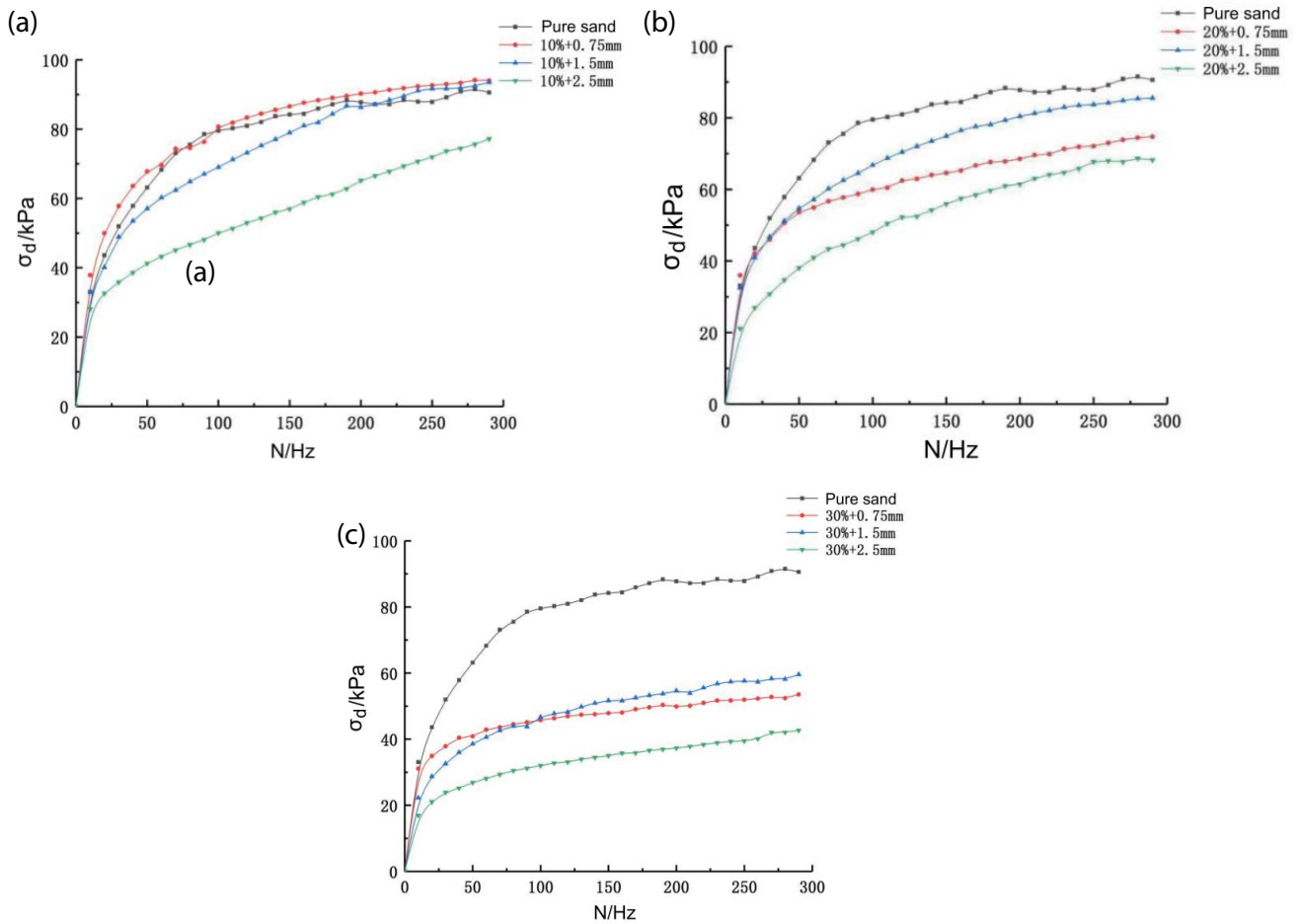


Fig. 4. Dynamic pore water pressure curve of samples with different dosages and particle sizes. Dosage of rubber particles (a) $R_f = 10\%$, (b) $R_f = 20\%$, and (c) $R_f = 30\%$.

permeability coefficient was increased, and the dynamic pore water pressure was dissipated more easily. Therefore, the anti-liquefaction performance was enhanced. However, adding small rubber particles into sand was equivalent to adding silt into sand, so the pores between sand were filled by silt, that is, the permeability coefficient of the samples was reduced and the pore water pressure was hard to dissipate, leading to poorer anti-liquefaction performance.

3.1.2. Effect of rubber dosage on anti-liquefaction performance of samples

According to Fig. 4c, with a rubber dosage of 30%, the dynamic pore water pressure reached 30–50 kPa and maintained stable at this level, which was far below the sample failure criterion. It can be seen that the samples are completely deprived of liquefying ability, and the liquefaction can be hardly observed. At this time, the rubber particles played a dominant role and served as the stressed skeleton of samples, while the sand particles filled the pores contacting rubber particles. All the analyses demonstrated that a certain amount of rubber particles mixed can remarkably improve the anti-liquefaction performance of samples. However, as the mixing amount exceeds a certain

level, the rubber particles in the samples occupy a dominant position, and the changed mechanical properties of samples result in no liquefaction.

3.2. Effect of confining pressure on anti-liquefaction performance of samples

To research the effect of confining pressure on the anti-liquefaction performance of RSM samples, three kinds of confining pressure with a gradient of 50 kPa (100, 150 and 200 kPa) were selected. The variation laws of the dynamic pore water pressure of the RSM samples under three different confining pressures are presented in Fig. 5. It was manifested that the higher the exerted confining pressure was, the lower the numerical value of dynamic pore water pressure in the stable stage would be. Thus, the samples were more difficult to be liquefied, that is, RSM samples with larger confining pressure possessed better anti-liquefaction performance. The analysis of the rule from a micro perspective indicated that in the case of greater confining pressure, the rubber-sand particles of the samples were arranged more densely, and the pores between particles was further decreased, thereby strengthening the anti-liquefaction performance of the samples.

Table 2
Effect of rubber particle size on anti-liquefaction performance of sand

D_r (mm)	$R_f = 10\%$		$R_f = 20\%$		$R_f = 30\%$	
	U_d (kPa)	Improvement rate (%)	U_d (kPa)	Improvement rate (%)	U_d (kPa)	Improvement rate (%)
0.75	94.4	0	74.5	17.2	53.5	40.5
1.5	92.6	0	86.1	4.4	59.4	33.9
2.5	78.4	12.8	68.5	23.8	42.7	52.6

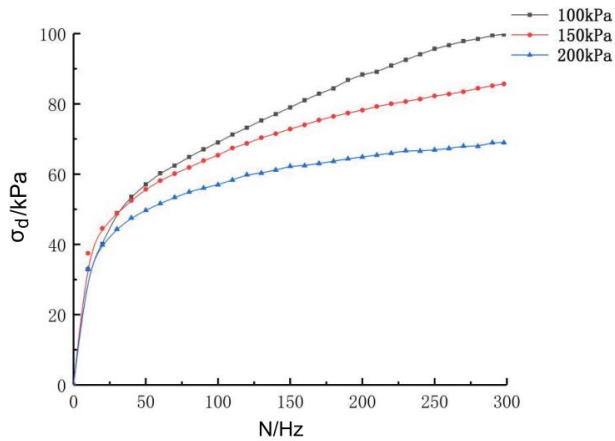


Fig. 5. Dynamic pore water pressure curve of samples with different confining pressure.

3.3. Effect of consolidation stress ratio on anti-liquefaction performance of samples

Dynamic Triaxial Tests were performed with three different consolidation stress ratios, namely $K = 1.0, 1.5$ and 2.0 , in order to research the law of the effect of consolidation stress ratio on the anti-liquefaction performance of samples. The criterion for completion of consolidation stabilization is that the back volume in the back-pressure sensor does not vary by more than 5 mm^3 , and the dynamic load is applied until the failure criterion is reached after consolidation.

The dynamic pore water pressure developmental curves of saturated RSM under different consolidation stress ratios are shown in Fig. 6. It was illustrated that the development law of dynamic pore water pressure varied with the increase of consolidation stress ratio, and the dynamic pore water pressure development curve of the samples with a large consolidation stress ratio tended to move downward. The anti-liquefaction performance of the samples increased with the increase of the consolidation stress ratio. In the same vibration times of 300, the dynamic pore water pressure of the samples with a consolidation stress ratio of $K = 1.0$ reached the test liquefaction criterion ($U_d = 90 \text{ kPa}$), while the dynamic pore water pressure of the samples with consolidation stress ratios of $K = 1.5, 2.0$ was only 46 and 25 kPa, respectively, under the vibration times of 300, far lower than the criterion of sample liquefaction. For microcosmic explanation of this phenomenon, when the consolidation stress ratio was $K = 1.5, 2.0$, the samples were subjected to a stress under larger confining pressure during consolidation, resulting in denser particle

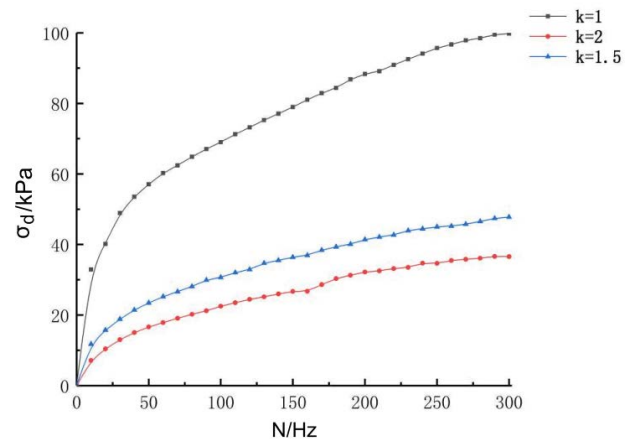


Fig. 6. Dynamic pore water pressure curve of samples with different consolidation stress ratios.

arrangement. When the consolidation stress ratio was larger than 1, shear stress was generated in the samples in the consolidation stage due to the presence of deviatoric stress. The shear stress then disturbed the particle arrangement in the samples and rearranged the rubber-sand particles, which could improve the anti-liquefaction performance of the samples, so liquefaction failure was not easy to occur in the samples under cyclic loading.

3.4. Function model of dynamic pore water pressure growth for RSM samples

Different types of soil samples have different types of dynamic pore water pressure growth curves. Therefore, the law of dynamic pore water pressure growth curves of given soil samples must be summarized on the basis of a large number of tests. In the light of the research and summary of scientific researchers in China and foreign countries on the development law of dynamic pore water pressure U_d in Dynamic Triaxial Tests, Seed [10] put forward earlier that the dynamic pore water pressure ratio U_d/σ'_3 and the vibration times ratio N/N_f conform to the increase law of anti-trigonometric function under the condition of constant-pressure consolidation [Eq. (5)]:

$$\frac{U_d}{\sigma_3} = \frac{2}{\pi} \arcsin \left(\frac{N}{N_f} \right)^{\frac{1}{6}} \quad (5)$$

where σ_3 : confining pressure applied in the test; θ : parameter related to the sample material; N_f : vibration times in the test.

Therefore, corresponding dynamic pore water pressure growth models were established based on the test results under the conditions of different rubber dosages, rubber particle sizes, confining pressures and consolidation stress ratios, and the pore water pressure ratio U_d/σ'_3 and the vibration times ratio N/N_f were obtained through the normalization of vibration times N and dynamic pore water pressure U_d . Zhang et al. [11–14] obtained three pore water pressure growth model functions on the basis of summarizing the development theories of dynamic pore water pressure U_d obtained by predecessors and carrying out a lot of Dynamic Triaxial Tests [Eqs. (6)–(9)].

$$U_d = U_f \left[\frac{1}{2} \left(1 - \cos \pi \frac{t}{t_f} \right) \right]^b \tag{6}$$

$$U_d = U_f \left(1 - e^{-\beta \frac{t}{t_f}} \right) \tag{7}$$

$$U_d = \frac{2}{\pi} U_f \sin^{-1} \left(\frac{t}{t_f} \right)^{\frac{1}{2a}} \tag{8}$$

$$\frac{U_d}{\sigma_3} = \frac{N / N_f}{a(N / N_f) + b} \tag{9}$$

where a, b : parameters related to sample materials; t_f : vibration time of the test; N_f : vibration times in the test; U_d : dynamic pore water pressure in the test.

In order to figure out the best fit function model, it was discovered *via* the Origin software that the hyperbolic function fitted best to the developmental curve of dynamic pore water pressure of RSM samples. Therefore, the hyperbolic function was selected to fit the developmental curve of dynamic pore water pressure of each group of RSM samples, as shown in Fig. 7. The relevant parameters a, b, R^2 of the hyperbolic curve fit model are shown in Table 3, where the fit function parameters a, b and error R^2 are compared and analyzed.

3.5. Analysis and discussion on composition micromechanism of rubber-sand particles

From the previous analysis of the results of Dynamic Triaxial Tests, it can be seen that the liquefaction of samples with a small dosage of rubber particles R_f is very similar to that of pure sand samples without rubber particles. When the dosage R_f was 10%, liquefaction occurred

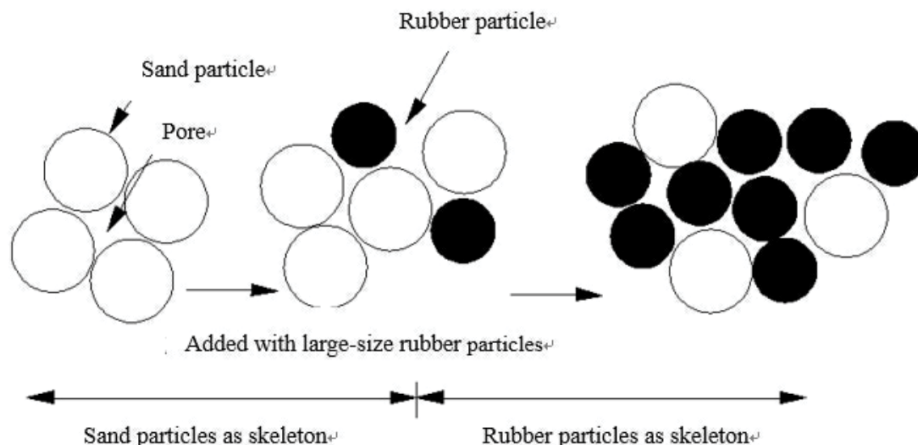


Fig. 7. Microscopic view of rubber-sand mixture samples with large-size rubber particles

Table 3
Summary of fit function parameters

Dosage R_f	Rubber particle size D_r (mm)	Coefficient a	Coefficient b	Error R^2
$R_f = 10\%$	0.75	1.0022	0.0741	0.9905
	1.5	0.9733	0.1280	0.9698
	2.5	1.1815	0.2196	0.9699
$R_f = 20\%$	0.75	1.3310	0.0828	0.9585
	1.5	1.0778	0.1168	0.9750
	2.5	1.2615	0.2323	0.9727
$R_f = 30\%$	0.75	1.8994	0.0684	0.9663
	1.5	1.5955	0.1573	0.9760
	2.5	2.3128	0.2172	0.9505

when the vibration times was 150, and a basically identical trend of the dynamic pore water pressure growth curves was observed between RSM samples and pure sand samples. With the gradual increase of dosage R_f (set as 20% and 30% in this test), the initial liquefaction vibration times of the RSM samples gradually increased. When the dosage of rubber particles was 20%, the initial liquefaction vibration times reached 250. When such a dosage reached 30% in the test, the dominant component of the RSM samples would be the rubber particles. Therefore, it was difficult to observe liquefaction during the test. With the same vibration times of 300, the dynamic pore water pressure of the samples was kept stable when it reached 52 kPa, and the numerical value of the dynamic pore water pressure was only half of the liquefaction failure criterion (the liquefaction criterion of the samples: dynamic pore water pressure $U_d =$ effective confining pressure $\sigma'_3 = 100$ kPa). Therefore, the addition of rubber particles into the pure sand samples could effectively improve the anti-liquefaction performance of pure sand, and the anti-liquefaction performance of RSM samples increased with the increase of the dosage of rubber particles.

The failure mode of the samples was also related to the dosage of rubber particles, and a small dosage of rubber particles might cause the RSM sample to show a tensile failure mode, similar to the tensile failure mode of pure sand samples. Different failure modes appeared with the increase of the dosage of rubber particles, when the dosage of rubber particles reached 30%. As for the compressive failure mode of the RSM, it was analyzed that when the pure sand is added with a large dosage of rubber particles, the sand particles control the stress property variations in the original pure sand samples, and the rubber-sand particles mutually control the stress property. The mechanical properties of the samples are close to those of the rubber particles as the skeleton when the dosage of rubber particles in the samples exceeds the critical value.

However, the larger dosage of rubber particles is not the better. When such a dosage reaches 30%, the mix ratio of the rubber particles and the sand for preparing the RSM sample is 112:52. Therefore, the rubber particles play a main role in the stressed skeleton of the sample, and the entire sample is deprived of the stress state structure of sand. Therefore, even though a large dosage of rubber particles can greatly improve the anti-liquefaction performance of pure sand samples, this practice does not conform to the actual conditions in engineering construction. Scholar Li et al. [15] studied the variation law of anti-liquefaction performance of RSM with different rubber dosages and found that there is a critical value for the rubber dosage in Dynamic Triaxial Tests, during which the sample will not liquefy basically when the dosage exceeds this value, and the critical value of such a dosage is determined as about 40% through a large number of tests. In this paper, the sample liquefaction in the Dynamic Triaxial Tests was hardly observed when the rubber dosage R_f was 30%, which is similar to the conclusion reached by the aforementioned scholars. In other words, the proper addition of rubber particles can effectively improve the anti-liquefaction performance of sand, and the effect of large-size rubber particles on anti-liquefaction performance of sand is particularly obvious [16].

Fig. 4 displays the dynamic pore water pressure curve of samples with different particle sizes and different dosages of rubber particles. It was found that the anti-liquefaction performance of the samples added with small-size rubber particles (0.75 mm) was generally greater than that of the samples added with large-size rubber particles (1.5 and 2.5 mm) (Fig. 4). The former was liquefied when the vibration times of cyclic loading reached about 150, and the dynamic pore water pressure of the later was 65 kPa when the strain was larger than 5% and the vibration times reached 300 (the liquefaction criterion of the samples: dynamic pore water pressure $U_d =$ effective confining pressure $\sigma'_3 = 100$ kPa). In comparison with the pure sand samples, the samples added with rubber particles had a larger compressive strain and a smaller variation in tensile strain after liquefaction, which is just opposite to the variation trend of strain after liquefaction of the pure sand samples. Therefore, the RSM samples have a stronger anti-liquefaction performance than pure sand samples. In terms of the increase rate of dynamic pore water pressure, the increase rate of the RSM samples with large-size rubber particles was obviously higher than that of the RSM samples with small-size rubber particles in the early stage of rapid growth of pore water pressure [17].

Scholars have analyzed this phenomenon from the microscopic perspective of particle composition [13]. Figs. 7 and 8 are the microscopic composition of RSM samples. This phenomenon can be attributed to two main reasons: First, when large-size rubber particles are added to the pure sand samples, it is equivalent to mixing gravel particles with elasticity into the sand, so the permeability coefficient of the RSM samples is increased accordingly. Under the cyclic loading, the dynamic pore water pressure is more likely to dissipate, so the anti-liquefaction performance of the samples is enhanced. Second, the added large-size rubber particles have a relatively low elastic modulus, so the RSM samples have a rebound effect under the cyclic loading, which makes the contact between rubber and sand particles closer. The microstructure of the RSM samples is more stable than that of the pure sand particles. In the initial stage of vibration, the pore water pressure increases rapidly and there is certain recoverable deformation capacity under the hydraulic dynamic effect among particles of the RSM samples, which weakens the accumulated rapid increase trend of pore water pressure. Therefore, the addition of large-size rubber particles can effectively enhance the anti-liquefaction performance of pure sand.

However, the structure of the pure sand samples added with small-size rubber particles is not the same as above. The addition of small-size rubber particles can be regarded as the addition of soil particles with lower elasticity to the pure sand. Therefore, the permeability coefficient of the RSM samples is reduced, so the pore water pressure does not dissipate in the initial vibration stage, the pore water pressure accumulates and increases rapidly, and liquefaction occurs. As a result, the anti-liquefaction performance of the RSM samples is reduced. It was manifested in the micro-diagram of RSM samples that the small-particle size rubber particles added filled the pores between sand particles, resulting in a decrease in the permeability coefficient of the samples, and the effect of small-size rubber particles was only to fill the

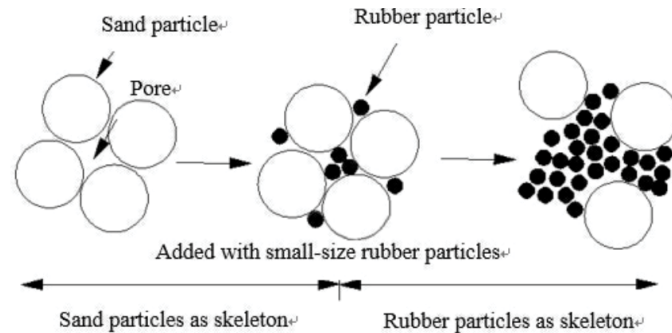


Fig. 8. Micro-diagram of rubber-sand mixture samples with small-size rubber particles.

pores, and the stressed skeleton of the whole sample was still controlled by sand particles. In case of a small dosage of rubber particles, the effect of small-size rubber particles is mainly to fill the pores between sand particles, and the stressed skeleton of the sample is mainly controlled by sand particles. However, in the case of adding large-size rubber particles under the condition of a high dosage of rubber particles, the contact between rubber and sand particles increased and the effect between rubber particles was greater than that between rubber and sand particles. Therefore, the stressed skeleton of the sample is altered and controlled by rubber particles instead of sand particles [18].

It can also be inferred from Fig. 8 that in the process of adding rubber particles with different particle sizes, there is a critical range of the dosage of rubber particles with smaller particle sizes R_f on the stressed skeleton of the pure sand sample, the stressed skeleton of the sample will be controlled by the rubber particles when the dosage of rubber particles exceeds this range, and the whole sample shows the mechanical properties of the rubber particles. The large-size rubber particles have no effect of filling the pores between particles and exist as stressed skeletons among particles of the RSM samples. Therefore, the anti-liquefaction performance of the pure sand samples can be significantly improved in case of a small dosage. When the dosage exceeds the critical range, the stressed skeleton of the samples is controlled by rubber particles, so it is rare to cause liquefaction.

4. Conclusion

A series of Dynamic Triaxial Tests were performed on the saturated RSM samples, and the effects of different rubber particle dosages and particle sizes on the dynamic pore water pressures of the samples were emphatically analyzed in this paper. The following conclusions were obtained:

- Through analysis and summarization of test data, the increase of dynamic pore water pressures of saturated pure sand and RSM in Dynamic Triaxial Tests could be divided into three stages, namely the stage of rapid growth of pore water pressure, the stage of uniform growth of pore water pressure, and the stage of stable pore water pressure. From the microscopic point of view, it is believed that when the sample is initially vibrated, the pores between the original particles are filled rapidly and the pore water pressure image shows a rapid

growth, the large pores between particles are initially filled, the small pores are gradually filled, and the pore water pressure enters the stage of uniform growth. When the pores between particles cannot be recompressed, the pore water pressure enters the stage of stable pore water pressure with only slight fluctuations.

- When different confining pressures and consolidation stress ratios are applied to the samples with the same dosage of rubber particles, it is found that the effects of confining pressure and consolidation stress ratio show the same law, namely the anti-liquefaction performance is enhanced with the increase of confining pressure or consolidation stress. A larger confining pressure and consolidation stress ratio can reduce the pores of the samples. Therefore, the anti-liquefaction performance of the samples under dynamic load is enhanced.
- Two influencing factors, dosage of rubber particles (0%, 10%, 20% and 30%) and rubber particle size (0.75, 1.5 and 2.5 mm), were comprehensively tested. It was found from the test results that the anti-liquefaction performance of pure sand is obviously enhanced by adding a certain dosage of rubber particles, and large-size rubber particles can effectively improve the anti-liquefaction performance of the samples. The variation law of dynamic pore water pressure of the samples added with 10% rubber particles is similar to that of pure sand, while the anti-liquefaction performance of samples added with 20% or 30% rubber particles is effectively improved. Therefore, the anti-liquefaction performance of the samples cannot be effectively improved in case of a small dosage of rubber particles. In terms of the dosage of rubber particles, there is a critical value due to different test conditions, and the mechanical properties of the samples vary, and no liquefaction occurs after this critical value is exceeded.
- In this paper, the hyperbolic function model was selected to fit the test data. It was found in the research that when the error R^2 approaches 100%, parameter a is substantially equal to 1, while parameter b fluctuates in the range of 0.06–0.2.

Acknowledgments

This study was supported by the Municipal Colleges and Universities Basic Scientific Research Business Expenses Project (X18199), the Beijing Municipal Education

Commission Scientific Research Project Science and Technology Plan General Project (Face Project) (Z18028) and School Research Fund Natural Science Project - Ad Hoc Fund (ZF17067).

References

- [1] S. Ahmed, A.K. Riaz, Temperature monitoring and compressibility measurement of a tire shred embankment: Winnipeg, Manitoba, Canada, Transp. Res. Record: J. Transp. Res. Board, 1808 (2002) 67–75.
- [2] T.B. Edil, A Review of Mechanical and Chemical Properties of Shredded Tires and Soil Mixtures, Recycled Materials in Geotechnics Sessions at ASCE Civil Engineering Conference and Exposition, Baltimore, Maryland, United States, 2004.
- [3] A. Edinçliler, A. Cagatay, Weak subgrade improvement with rubber fibre inclusions, Geosynth. Int., 20 (2013) 39–46.
- [4] L.-H. Li, H.-L. Xiao, H.M. Tang, Q. Ma, H. Chen, L. Sun, Shear performance optimizing of tire shred-sand mixture, Rock Soil Mech., 34 (2013) 1063–1067.
- [5] M.S. Mashiri, J.S. Vinod, M.N. Sheikh, Constitutive model for sand–tire chip mixture, Int. J. Geomech., 16 (2015) 04015022, doi: 10.1061/(ASCE)GM.1943-5622.0000472.
- [6] M.X. Ng, T.C. Tham, S.P. Ong, C.L. Law, Drying kinetics of technical specified rubber, Inf. Process. Agric., 2 (2015) 64–71.
- [7] S. Chacko, J. Kurian, C. Ravichandran, S.M. Vairavel, K. Kumar, An assessment of water yield ecosystem services in Periyar Tiger Reserve, Southern Western Ghats of India, Geol. Ecol. Landscapes, 5 (2021) 32–39.
- [8] S.M. Al-Gorany, S.Z. Al-Abachi, A.I. Arif, E.E. Abogllida, E.H. Al-Abdeli, Preliminary phytochemical screening and GC-MS analysis of bioactive constituents in the ethanolic extract of empty fruit bunches, J. Clean WAS, 4 (2020) 70–74.
- [9] B. Tiwari, B. Ajmera, S. Moubayed, A. Lemmon, K. Styler, Soil Modification with Shredded Rubber Tires, GeoCongress 2012, Oakland, California, United States, 2012, pp. 3701–3708.
- [10] W. Zhu, M.-D. Li, C.-L. Zhang, H. Li, Optimum moisture content of sand EPS beads mixed lightweight soil, Chin. J. Geotech. Eng., 31 (2009) 21–25.
- [11] K. Sankaran, P. Manoharan, S.S. Reka, S. Chattopadhyay, A brief insight into the prediction of water vapor transmissibility in highly impermeable hybrid nanocomposites based on bromobutyl/epichlorohydrin rubber blends, Open Chem., 16 (2018) 1207–1213.
- [12] H. Bolton Seed, K.L. Lee, Liquefaction of saturated sands during cyclic loading, J. Soil Mech. Found. Div., 92 (1966) 105–134.
- [13] J.M. Zhang, D.Y. Xie, A practical calculation method for increase of pore water pressure of saturated sand under vibration, J. Hydraul. Eng., 8 (1991) 45–51.
- [14] H.-K. Kim, J.C. Santamarina, Sand–rubber mixtures (large rubber chips), Can. Geotech. J., 45 (2008) 1457–1466.
- [15] J.R. Valdes, T. Matthew Evans, Sand–rubber mixtures: experiments and numerical simulations, Can. Geotech. J., 45 (2008) 588–595.
- [16] M.A. Shahin, T. Mardesic, H.R. Nikraz, Geotechnical characteristics of bauxite residue sand mixed with crumbed rubber from recycled car tires, J. Geoeng., 6 (2011) 63–72.
- [17] B. Li, M.-S. Huang, Dynamic Triaxial Tests on liquefaction characteristics of rubber-sand mixture, Rock Soil Mech., 38 (2017) 1343–1349.
- [18] R.A.G. Whba, L. TianKhoon, M.S. Su'ait, M.Y.A. Rahman, A. Ahmad, Influence of binary lithium salts on 49% poly(methyl methacrylate) grafted natural rubber based solid polymer electrolytes, Arabian J. Chem., 13 (2020) 3351–3361.